

Spectral Function for the Anderson Model based on Nonequilibrium Perturbation Theory

Mami Hamasaki [§]

Department of Physics, Kyoto University, Kyoto, Japan

Abstract. The spectral function based on the nonequilibrium perturbation theory up to the fourth-order is shown for the symmetric Anderson model and the characteristic of the Kondo resonance is investigated for nonequilibrium state caused by bias voltage. The third-order and the fourth-order contributions to the retarded and advanced self-energies are formulated and then it is proved that the generalized nonequilibrium (real-time) perturbative expansion can be connected with the Matubara imaginary-time perturbative expansion for equilibrium. As the numerical results on spectral function, the Kondo peak fades for bias voltage exceeding the Kondo temperature; this characteristic has been observed by the recent experiment. The present results suggest that the Kondo resonance can be destroyed owing to fluctuation of the Fermi level in nonequilibrium state

[§] E-mail address: hamasaki@scphys.kyoto-u.ac.jp

1. Introduction

The Kondo effect [1] was discovered forty years ago and after that, the Kondo physics has been clarified from Landau's Fermi liquid theory [2], the renormalization group [3], scaling [4], etc.. Besides, generalized Kondo problem, that of more than one channel or one impurity has been investigated. [5, 6] Then, the Kondo effect in electron transport through a quantum dot has been predicted theoretically at the end of 1980s [7] and after a decade, this phenomenon has been observed. [8] The Kondo effect has been studied theoretically using the Anderson model and the predictions have been confirmed experimentally. In the Kondo regime, the conductance has been observed to reach the unitarity limit and the Kondo temperature estimated from observation [9] is in excellent agreement with the expression derived using the Anderson model. [10] Furthermore, the Kondo effect in a quantum dot has been studied for nonequilibrium system where the bias voltage is applied. [11] In some theoretical work, for instance, Refs. [12-15] it is insisted that the Kondo peak in the spectral function splits into two peaks, each of which is pinned to the left and right chemical potentials in the presence of bias voltage. In experiment on a carbon nanotube quantum dot, it has been observed that the Kondo effect is suppressed when source-drain bias voltage is comparable to the Kondo temperature. [16] Moreover, the Kondo peak splitting in differential conductance takes place in the absence of magnetic field; this is explained as the results of coupling of the dot to a ferromagnetic impurity. [16]

The basic idea on the nonequilibrium perturbation theory grounded on the time-contour which starts and ends at $t = -\infty$ via $t = \infty$ has been proposed by Schwinger. [17] After that, the frame of the nonequilibrium perturbation theory has been built up using the nonequilibrium Green's functions introduced on the basis of the time-contour by Keldysh. [18] However, the general formalism for the nonequilibrium perturbation theory has not been established yet; much work has been carried out in various manners. Hershfield *et al.* have extended perturbation theory for equilibrium [19] based on the Fermi liquid theory [2] to nonequilibrium system and have shown that for bias voltage higher than the Kondo temperature, the Kondo resonance disappears in the spectral function with the second-order self-energy for the Anderson model; [20] moreover, the related work grounded on the Fermi liquid theory has been done. [21] Nevertheless, for nonequilibrium perturbation theory, the perturbative expansion higher than the second-order has ever been left unsolved and thus, the characteristic of the spectral function for approximation higher than the second-order has not been clarified.

The present work is performed in the generalized formalism for the nonequilibrium perturbation theory. The spectral function with perturbation up to the fourth-order is shown for the Anderson model and the characteristic of the Kondo resonance is investigated for nonequilibrium state caused by applied dc voltage. It is required to introduce the improvement of the definition in the Keldysh formalism and then the third- and the fourth-order contributions to the retarded and advanced self-energies are

formulated. As the result, it is demonstrated that the generalized nonequilibrium (real-time) perturbative expansion can be connected with the Matubara imaginary-time perturbative expansion for equilibrium. The expressions for the third-order self-energy at equilibrium are in agreement with those derived from the Matubara imaginary-time perturbative expansion for equilibrium and analytical continuity by Zlatić *et al.* [22]. For the fourth-order self-energy at equilibrium and the electron-hole symmetry, the asymptotic behavior at low energy agrees approximately with the exact results based on the Bethe ansatz method. [23] As numerical results on spectral function within the approximation up to the fourth-order, high and sharp peaks rise at energy levels of the atomic limit for equilibrium and electron correlation large enough. Besides, the Kondo peak fades for bias voltage exceeding the Kondo temperature. This characteristic has been observed by the recent experiment. [16] The results suggest that the Kondo resonance can be destroyed because of fluctuation of the Fermi level on the impurity in nonequilibrium state.

2. Model and Nonequilibrium Perturbation Theory

We consider nonequilibrium stationary state. The system is described by the Anderson model connected to leads. The impurity with on-site energy E_0 and the Coulomb interaction U is connected to the left and right leads by the mixing matrix elements, v_L and v_R . The Anderson Hamiltonian is given by

$$\begin{aligned}
 \mathcal{H} = & E_0 \sum_{\sigma} \hat{n}_{d\sigma} + \mu_L \sum_{\sigma} \hat{n}_{L\sigma} + \mu_R \sum_{\sigma} \hat{n}_{R\sigma} + U(\hat{n}_{d\uparrow} - \langle \hat{n}_{d\uparrow} \rangle)(\hat{n}_{d\downarrow} - \langle \hat{n}_{d\downarrow} \rangle) \\
 & - \sum_{\sigma} v_L (\hat{d}_{\sigma}^{\dagger} \hat{c}_{L\sigma} + \text{H.c.}) - \sum_{\sigma} v_R (\hat{d}_{\sigma}^{\dagger} \hat{c}_{R\sigma} + \text{H.c.}).
 \end{aligned} \tag{1}$$

\hat{d}^{\dagger} (\hat{d}) is creation (annihilation) operator for electron on the impurity, and \hat{c}_L^{\dagger} and \hat{c}_R^{\dagger} (\hat{c}_L and \hat{c}_R) are creation (annihilation) operators in the left and right leads, respectively. σ is index for spin. The chemical potentials in the isolated left and right leads are μ_L and μ_R , respectively. Therefore, the applied voltage is defined by $eV \equiv \mu_L - \mu_R$.

2.1. Nonequilibrium Green's Functions and Perturbative Expansion on Real-Time

Four nonequilibrium Green's functions in the Heisenberg representation are introduced by

$$G^{--}(t_1, t_2) \equiv -i \langle \text{T} \hat{d}(t_1) \hat{d}^{\dagger}(t_2) \rangle, \tag{2}$$

$$G^{++}(t_1, t_2) \equiv -i \langle \tilde{\text{T}} \hat{d}(t_1) \hat{d}^{\dagger}(t_2) \rangle, \tag{3}$$

$$G^{>}(t_1, t_2) \equiv -i \langle \hat{d}(t_1) \hat{d}^{\dagger}(t_2) \rangle, \tag{4}$$

$$G^{<}(t_1, t_2) \equiv i \langle \hat{d}^{\dagger}(t_2) \hat{d}(t_1) \rangle. \tag{5}$$

Here, the time ordering operator T arranges in chronological order and $\tilde{\text{T}}$ is the anti time ordering operator which arranges in the reverse of chronological order. The angular brackets denote thermal average in nonequilibrium. Straightforwardly, $G^{--}(t) =$

$\theta(t)G^>(t) + \theta(-t)G^<(t)$, $G^{++}(t) = \theta(t)G^<(t) + \theta(-t)G^>(t)$. The Dyson's equation in the Keldysh formalism is given by

$$\mathbf{G} = \mathbf{g} + \mathbf{g} \Sigma \mathbf{G}, \quad (6)$$

where

$$\mathbf{G} = \begin{bmatrix} G^{--} & G^< \\ G^> & G^{++} \end{bmatrix}, \quad \Sigma = \begin{bmatrix} \Sigma^{--} & \Sigma^< \\ \Sigma^> & \Sigma^{++} \end{bmatrix}.$$

Here, \mathbf{g} is unperturbed Green's functions. In addition, according to the definition, the retarded and advanced Green's functions are given by

$$G^r(t_1, t_2) \equiv -i\theta(t_1 - t_2)\langle\{\hat{d}(t_1), \hat{d}^\dagger(t_2)\}\rangle, \quad (7)$$

$$G^a(t_1, t_2) \equiv i\theta(t_2 - t_1)\langle\{\hat{d}(t_1), \hat{d}^\dagger(t_2)\}\rangle. \quad (8)$$

Here, the curly brackets denote anticommutator. $G^r(t) = \theta(t)[G^>(t) - G^<(t)]$, $G^a(t) = \theta(-t)[G^<(t) - G^>(t)]$. The Dyson's equations are given by

$$G^r = g^r + g^r \Sigma^r G^r, \quad (9)$$

$$G^a = g^a + g^a \Sigma^a G^a. \quad (10)$$

We consider that the band-width of left and right leads is large infinitely, so that the coupling functions, Γ_L and Γ_R can be taken to be independent of energy, E . On-site energy E_0 is set canceling with the Hartree term, *i.e.* the first-order contribution to self-energy for electron correlation: $\Sigma_\sigma^{r(1)}(E) = \Sigma_\sigma^{a(1)}(E) = U\langle n_{-\sigma} \rangle$. Accordingly, the Fourier components of the noninteracting (unperturbed) Green's functions reduce to

$$g^r(E) = \frac{1}{E + i\Gamma}, \quad (11)$$

$$g^a(E) = \frac{1}{E - i\Gamma}, \quad (12)$$

where $\Gamma = (\Gamma_L + \Gamma_R)/2$. Hence, the inverse Fourier components can be written by $g^r(t) = -i\theta(t)e^{-\Gamma t}$ and $g^a(t) = i\theta(-t)e^{\Gamma t}$. In addition,

$$g^<(E) = g^r(E) [if_L(E)\Gamma_L + if_R(E)\Gamma_R] g^a(E), \quad (13)$$

$$g^>(E) = g^r(E) [i(1 - f_L(E))\Gamma_L + i(1 - f_R(E))\Gamma_R] g^a(E). \quad (14)$$

f_L and f_R are the Fermi distribution functions in the isolated left and right leads, respectively. The nonequilibrium state are represented as the superposition of the left and right leads.

A thermal average can be obtained on the basis of the nonequilibrium perturbation theory. [17, 18, 21, 24, 25, 26, 27] When the time evolution of the state is irreversible, then, the state at $t = \infty$ can not be well-defined. Therefore, the time evolution is performed along the real-time contour which starts and ends at $t = -\infty$, as illustrated in Fig. 1. S matrix is defined by

$$\begin{aligned} \mathcal{S}(t, t_0) &= 1 + \sum_{n=1}^{\infty} \frac{1}{n!} \left(\frac{-i}{\hbar}\right)^n \int_{t_0}^t dt_1 \dots \int_{t_0}^t dt_n T [\tilde{\mathcal{H}}_I(t_1) \dots \tilde{\mathcal{H}}_I(t_n)] \\ &= T \left[\exp \left\{ \frac{-i}{\hbar} \int_{t_0}^t dt' \tilde{\mathcal{H}}_I(t') \right\} \right], \end{aligned} \quad (15)$$

$$\mathcal{S}(t, t_0)^\dagger = \mathcal{S}(t_0, t) = \tilde{T} \left[\exp \left\{ \frac{i}{\hbar} \int_{t_0}^t dt' \tilde{\mathcal{H}}_I(t') \right\} \right]. \quad (16)$$

Here $\tilde{\mathcal{H}}_I$ is perturbation term in interaction representation. The thermal average in the Heisenberg representation at $t = 0$ can be obtained, for example by [21]

$$\begin{aligned} & \langle T A(t) B(t') \rangle \\ & \equiv \text{Tr}[\varrho(0) T A(t) B(t')] \\ & = \text{Tr}[\tilde{\varrho}(-\infty) \mathcal{S}(-\infty, 0) T A(t) B(t') \mathcal{S}(0, -\infty)] \\ & = \text{Tr}[\tilde{\varrho}(-\infty) \mathcal{S}(-\infty, \infty) \{ T \mathcal{S}(\infty, -\infty) \tilde{A}(t^-) \tilde{B}(t'^-) \}] \\ & = \sum_{n=1}^{\infty} \sum_{m=1}^{\infty} \frac{1}{n!} \frac{1}{m!} \left(\frac{i}{\hbar} \right)^n \left(\frac{-i}{\hbar} \right)^m \int_{-\infty}^{\infty} dt_1 \dots \int_{-\infty}^{\infty} dt_n \int_{-\infty}^{\infty} dt'_1 \dots \int_{-\infty}^{\infty} dt'_m \\ & \quad \times \langle \left\{ \tilde{T} \tilde{\mathcal{H}}_I(t_1^+) \dots \tilde{\mathcal{H}}_I(t_n^+) \right\} \left\{ T \tilde{\mathcal{H}}_I(t_1'^-) \dots \tilde{\mathcal{H}}_I(t_m'^-) \tilde{A}(t^-) \tilde{B}(t'^-) \right\} \rangle_{av}, \end{aligned}$$

where $\langle \dots \rangle_{av} = \text{Tr}[\tilde{\varrho}(-\infty) \dots]$. Here, $\varrho(t)$ is the statistical operator (density matrix) in the Heisenberg representation and $\tilde{\varrho}(t)$ is in interaction representation. \tilde{A} denotes an arbitrary operator in interaction representation.

2.2. Self-Energy for Electron Correlation

After the perturbative expansion is executed, the retarded and advanced self-energies are formulated. It is essential to introduce the improvement of the definition in the Keldysh formalism, as follows:

$$\Sigma^r(t) = [\Sigma^{--}(t) + \Sigma^<(t)]\theta(t) = -[\Sigma^{++}(t) + \Sigma^>(t)]\theta(t), \quad (17)$$

$$\Sigma^a(t) = [\Sigma^{--}(t) + \Sigma^>(t)]\theta(-t) = -[\Sigma^{++}(t) + \Sigma^<(t)]\theta(-t). \quad (18)$$

These are because $\Sigma^{--}(t) \neq \Sigma^{--}(-t)$, $\Sigma^{++}(t) \neq \Sigma^{++}(-t)$, $\Sigma^<(t) \neq \Sigma^<(-t)$ and $\Sigma^>(t) \neq \Sigma^>(-t)$, generally. (Nonetheless, these are missing in the Keldysh formalism.) For this reason, the retarded and advanced self-energies can not be written in energy representation; as a consequence, these are expressed as the Fourier transformation of time representation. The second-order self-energy is written by

$$\begin{aligned} \Sigma^{r(2)}(E) &= U^2 \int_0^\infty dt_1 e^{iEt_1} \begin{bmatrix} g^>(t_1) g^>(t_1) g^<(-t_1) \\ -g^<(t_1) g^<(t_1) g^>(-t_1) \end{bmatrix} \\ &= U^2 \int_0^\infty dt_1 e^{iEt_1} \begin{bmatrix} g^\pm(t_1) g^>(t_1) g^<(-t_1) \\ +g^<(t_1) g^\pm(t_1) g^>(-t_1) \\ +g^<(t_1) g^>(t_1) g^\pm(-t_1) \end{bmatrix}, \end{aligned} \quad (19)$$

$$\begin{aligned} \Sigma^{a(2)}(E) &= U^2 \int_{-\infty}^0 dt_1 e^{iEt_1} \begin{bmatrix} g^<(t_1) g^<(t_1) g^>(-t_1) \\ -g^>(t_1) g^>(t_1) g^<(-t_1) \end{bmatrix} \\ &= U^2 \int_{-\infty}^0 dt_1 e^{iEt_1} \begin{bmatrix} g^\pm(t_1) g^>(t_1) g^<(-t_1) \\ +g^<(t_1) g^\pm(t_1) g^>(-t_1) \\ +g^<(t_1) g^>(t_1) g^\pm(-t_1) \end{bmatrix}. \end{aligned} \quad (20)$$

Here $g^\pm(t) = g^r(t) + g^a(t)$, that is, $g^+(t) = g^r(t) = -i\theta(t)e^{-\Gamma t}$ for $t \geq 0$ and $g^-(t) = g^a(t) = i\theta(-t)e^{\Gamma t}$ for $t < 0$. Additionally, $g^<(t)$ and $g^>(t)$ are the inverse Fourier

components of Eqs. (13) and (14). Figure 2 shows the diagram for the second-order self-energy. In the symmetric equilibrium case, the asymptotic behavior at low energy is expressed by

$$\Sigma^{r(2)}(E) \simeq -\Gamma \left(3 - \frac{\pi^2}{4}\right) \left(\frac{U}{\pi\Gamma}\right)^2 \frac{E}{\Gamma} - i\frac{\Gamma}{2} \left(\frac{U}{\pi\Gamma}\right)^2 \left(\frac{E}{\Gamma}\right)^2, \quad (21)$$

the exact results based on the Bethe ansatz method. [23, 28]

The third-order contribution to the self-energy is shown. The terms corresponding to the diagram denoted in Fig. 3(a) are expressed by

$$\begin{aligned} \Sigma_{pp}^{r(3)}(E) &= U^3 \int_0^\infty dt_1 \int_{-\infty}^\infty dt_2 e^{iEt_1} \left[\begin{array}{c} g^<(-t_1)g^>(t_1 - t_2)g^>(t_1 - t_2) \\ -g^>(-t_1)g^<(t_1 - t_2)g^<(t_1 - t_2) \end{array} \right] \\ &\times \left[\begin{array}{c} g^\pm(t_2)g^>(t_2) + g^<(t_2)g^\pm(t_2) \end{array} \right], \end{aligned} \quad (22)$$

$$\begin{aligned} \Sigma_{pp}^{a(3)}(E) &= U^3 \int_{-\infty}^0 dt_1 \int_{-\infty}^\infty dt_2 e^{iEt_1} \left[\begin{array}{c} g^>(-t_1)g^<(t_1 - t_2)g^<(t_1 - t_2) \\ -g^<(-t_1)g^>(t_1 - t_2)g^>(t_1 - t_2) \end{array} \right] \\ &\times \left[\begin{array}{c} g^\pm(t_2)g^>(t_2) + g^<(t_2)g^\pm(t_2) \end{array} \right]. \end{aligned} \quad (23)$$

Figure 3(b) illustrates the diagram for the following terms:

$$\begin{aligned} \Sigma_{ph}^{r(3)}(E) &= U^3 \int_0^\infty dt_1 \int_{-\infty}^\infty dt_2 e^{iEt_1} \left[\begin{array}{c} g^>(t_1)g^>(t_1 - t_2)g^<(t_2 - t_1) \\ -g^<(t_1)g^<(t_1 - t_2)g^>(t_2 - t_1) \end{array} \right] \\ &\times \left[\begin{array}{c} g^\pm(t_2)g^<(-t_2) + g^<(t_2)g^\pm(-t_2) \end{array} \right], \end{aligned} \quad (24)$$

$$\begin{aligned} \Sigma_{ph}^{a(3)}(E) &= U^3 \int_{-\infty}^0 dt_1 \int_{-\infty}^\infty dt_2 e^{iEt_1} \left[\begin{array}{c} g^<(t_1)g^<(t_1 - t_2)g^>(t_2 - t_1) \\ -g^>(t_1)g^>(t_1 - t_2)g^<(t_2 - t_1) \end{array} \right] \\ &\times \left[\begin{array}{c} g^\pm(t_2)g^<(-t_2) + g^<(t_2)g^\pm(-t_2) \end{array} \right]. \end{aligned} \quad (25)$$

Equations (22)-(25) at equilibrium agree with those derived from the Matubara imaginary-time perturbative expansion for equilibrium and analytical continuity by Zlatić *et al.* [22]

Furthermore, the fourth-order contribution to the self-energy is formulated. (See Appendix.) The twelve terms for the proper fourth-order self-energy can be divided into four groups, each of which comprises three terms. The four groups correspond to the diagrams denoted in Figs. 4 (a)-(c), Figs. 4 (d)-(f), Figs. 4 (g)-(i), and Figs. 4 (j)-(l), respectively. For symmetric Anderson model at equilibrium, the asymptotic behavior at low energy is approximately in agreement with those based on the Bethe ansatz method [23]:

$$\Sigma^{r(4)}(E) \simeq -\Gamma \left(105 - \frac{45\pi^2}{4} + \frac{\pi^4}{16}\right) \left(\frac{U}{\pi\Gamma}\right)^4 \frac{E}{\Gamma} - i\frac{\Gamma}{2} \left(30 - 3\pi^2\right) \left(\frac{U}{\pi\Gamma}\right)^4 \left(\frac{E}{\Gamma}\right)^2. \quad (26)$$

3. Numerical Results and Discussion

3.1. Self-Energy

The third-order terms, Eqs. (22)-(25) cancel under electron-hole symmetry not only at equilibrium but also at nonequilibrium: $\Sigma_{ph}^{r(3)}(E) = -\Sigma_{pp}^{r(3)}(E)$ and $\Sigma_{ph}^{a(3)}(E) = -\Sigma_{pp}^{a(3)}(E)$. As a consequence, the third-order contribution to self-energy vanishes in the symmetric case. In this connection, the results of Refs. [19, 28, 29] show that all odd-order contributions except the Hartree term vanish at equilibrium in the symmetric single-impurity Anderson model; probably, it is just the same with nonequilibrium state. On the other hand, the third-order terms contribute to the asymmetric system where electron-hole symmetry breaks and furthermore, the third-order terms for spin-up and for spin-down contribute respectively for the spin degeneracy being lifted, e.g. by the magnetic field. For the fourth-order contribution, three terms which constitute each of four groups contribute equivalently under electron-hole symmetry. Moreover, to the asymmetric system, the terms brought by the diagrams of Figs. 4(a) and 4(b) contribute equivalently and the terms by the diagrams of Figs. 4(j) and 4(k) make equivalent contribution, and the rest, the eight terms contribute respectively. Further, the twenty-four terms for spin-up and spin-down take effect severally, for instance, in the presence of magnetic field.

The second-order and the fourth-order contributions to self-energy for zero temperature symmetric Anderson model are shown in Figs. 5(a) and 5(b) and in Figs. 6(a) and 6(b), respectively. Equation (21) represents the curves around $E = 0$ denoted by solid line in Figs. 5(a) and 5(b), respectively, and Equation (26) represents approximately those shown in Figs. 6(a) and 6(b), respectively. The fourth-order contribution oscillates as a function of energy more than the second-order. When the voltage, eV/Γ exceeds ~ 2.0 , the behavior changes distinctly and comes to present striking contrasts to that for the second-order contribution. Especially, the curve for the imaginary part of the fourth-order contribution rises up with maximum at $E = 0$. On the other hand, for the second-order contribution, a valley appears with minimum at energy of zero—it is quite the contrary. Moreover, from the these results, it is expected that the sixth-order contribution to imaginary part of self-energy has minimum at $E = 0$. Because of these, the perturbative expansion is hard to converge for $eV/\Gamma > \sim 2.0$, as mentioned later.

Besides, the current conservation is mentioned. In Ref. [20], it is shown that the continuity of current entering and leaving the impurity stands exactly at any strength of U within the approximation up to the second-order for the symmetric single-impurity Anderson model. In comparison of Figs. 6(a) and 6(b) with Figs. 5(a) and 5(b), it is found that curves of fourth-order self-energy have the symmetry similar to those of the second-order. From this, it is anticipated that the current conservation are satisfied perfectly within approximation up to the fourth-order in the single-impurity system where electron-hole symmetry holds. The continuity of current can be satisfied perfectly in single-impurity system as far as electron-hole symmetry stands. On the other hand,

current comes to fail to be conserved with increasing U in asymmetric single-impurity case and in two-impurity case.

3.2. Spectral Function

The spectral function with the second-order self-energy is as generally known. It is plotted for $U/\Gamma = 10.0$ and zero temperature in Fig. 7. For equilibrium, the Kondo peak at energy of zero is very sharp and the two-side broad peaks appear at $E \simeq \pm U/2$. The curve for $eV = 0$ is identical with that shown in Ref. [28]. As eV becomes higher than the Kondo temperature, $k_B T_K$ [30], the Kondo peak becomes lower and finally vanishes, while the two-side broad peaks rise at $E \simeq \pm U/2$.

Figure 8(a) shows the spectral function with the self-energy up to the fourth-order for equilibrium and zero temperature. With strengthening U , two-side narrow peaks come to occur in the vicinity of $E = \pm U/2$ in addition to the Kondo peak. At U large enough, the Kondo peak becomes very acute and two-side narrow peaks rise higher and sharpen; the energy levels for the atomic limit are produced distinctly. The fourth-order contribution takes effect upon the peak structure owing to their curves oscillating as a function of energy. However, in Ref. [28], it is said that the fourth-order contribution at equilibrium is so small in comparison with that of the second-order that the effect of the fourth-order self-energy is ignorable; this implies that the contributions higher than the second-order are of no effect at equilibrium symmetric Anderson model. As the numerical results in Ref. [28], it appears that curves of the fourth-order contribution are flat wholly. Actually, nonetheless, curves of the fourth-order contribution must oscillate as a function of energy more than the second-order. (The higher-order contribution is, the more the curves of the contribution must oscillate as a function of energy.) As a consequence, the fourth-order contribution can work on the peak structure effectively.

For the present approximation up to the fourth-order, the Kondo peak at $E = 0$ reaches the unitarity limit and the charge, $\langle n \rangle$ corresponds to 1/2, that is, the Friedel sum rule is correctly satisfied: [31]

$$\rho(E_f) = \sin^2(\pi\langle n \rangle)/\pi\Gamma, \quad (27)$$

where $\rho(E_f)$ is the local density of states at the Fermi energy. Here, the discussions should be made on the ranges of U in which the present approximation up to the fourth-order stands. From the results, it is found that the approximation within the fourth-order holds up to $U/\Gamma \sim 5.0$ and is beyond the validity for $U/\Gamma > \sim 6.0$. In addition, the curve for imaginary part of the fourth-order contribution is positive partly, as shown in Fig. 6(b) and as a consequence, the curve of the spectral function becomes negative partly for too large U . In such a case, the present approximation is out of validity.

Next, the results for nonequilibrium and zero temperature are shown. The expression for the Friedel sum rule, Eq. (27) does not stand for nonequilibrium, since the charge can not be expressed with respect to the local density of states. However, the Kondo peak reaches the unitarity limit and $\langle n \rangle = 1/2$ in the symmetric and noninteracting case. The spectral functions with the self-energy up to the fourth-order

are plotted for $eV/\Gamma = 0.5$ and $eV/\Gamma = 1.0$ in Figs. 8(b) and 8(c), respectively. When U is strengthened and eV exceeds $k_B T_K$ (approximately, $k_B T_K/\Gamma \sim 0.5$ for $U/\Gamma = 3.5$ and $k_B T_K/\Gamma \sim 0.3$ for $U/\Gamma = 5.0$), the Kondo peak for $eV/\Gamma = 0.5$ falls in and instead, the two-side narrow peaks remain to sharpen in the vicinity of $E = \pm U/2$. For $eV/\Gamma = 1.0$, the Kondo peak becomes broad and disappears for U large enough. The two-side peaks are generated small in the vicinity of $E = \pm U/2$. The Kondo resonance is quite broken for bias voltage exceeding the Kondo temperature; this accords with the recent experimental result that the Kondo effect is suppressed at $eV \sim k_B T_K$. [16] For $eV/\Gamma > \sim 2.0$, the Kondo peak does not lower even when eV is much larger than $k_B T_K$. The perturbative expansion is hard to converge owing to the imaginary part of the self-energy for $eV/\Gamma > \sim 2.0$, as described before; thereby, the higher-order contribution to self-energy is probably required for high voltage. In the present work, the effects of the electron correlation and nonequilibrium are dealt with and it is concluded that the destruction of the Kondo resonance is ascribed to the effect of nonequilibrium caused by bias voltage. For finite voltage, the impurity is in nonequilibrium state; the Fermi level on the impurity fluctuates owing to nonequilibrium, from the phenomenological point of view. The present results suggest that the Kondo resonance can be destroyed because of fluctuation of the Fermi level in nonequilibrium state.

The real system of the nonequilibrium state induced by bias voltage can be explained as follows: when the mixing between the impurity and the leads is large enough and the impurity is in nonequilibrium state, the Fermi level on the impurity is not fixed in nonequilibrium state, that is, the Fermi level fluctuates ranging from μ_R to μ_L , approximately. The average of the Fermi level is within the range from μ_R to μ_L , approximately. On the impurity in nonequilibrium state, there are not two different energy levels separately induced by μ_L and μ_R , respectively. Hence, in the density of states, the Kondo peak can not split into two peaks, each of which is pinned to the left and right chemical potentials.

As the numerical results in Refs. [12-14] of noncrossing approximation method (NCA) or equations of motion method (EOM), the Kondo peak splitting due to dc voltage appears in the spectral function. As found from expressions for these formalism, the state of the superposition of the left and right leads is broken partly. This is because the formalism of the nonequilibrium perturbation theory is modulated in the process of these methods. The nonequilibrium state mentioned above is not assumed in these cases.

Furthermore, we consider the system that the magnetic field is applied to the impurity. Then, the Zeeman term of the impurity, $-BS_Z$ (B is magnetic field) is added to the present Hamiltonian. Magnetization for spin 1/2 is written by $M = \langle S_Z \rangle = \frac{1}{2}(\langle \hat{n}_{d\uparrow} \rangle - \langle \hat{n}_{d\downarrow} \rangle) = \frac{1}{4\pi i} \int dE [G_{\uparrow}^<(E) - G_{\downarrow}^<(E)]$. For simplification, it is assumed that it is noninteracting ($U = 0$). In zero temperature limit ($T \rightarrow 0$), the expressions for magnetization M and susceptibility χ at equilibrium ($eV = 0$) reduce to $M(B) = \frac{1}{\pi} \arctan \left(\frac{B}{\Gamma} \right)$ and $\chi(B) = \frac{1}{\pi} \frac{\Gamma}{B^2 + \Gamma^2}$. In the nonequilibrium state ($\mu_L = -\mu_R = eV/2$, $\Gamma_L = \Gamma_R = \Gamma$), $M(B, eV) = \frac{1}{2\pi} \left[\arctan \left(\frac{B+eV/2}{\Gamma} \right) + \arctan \left(\frac{B-eV/2}{\Gamma} \right) \right]$

and $\chi(B, eV) = \frac{\Gamma[B^2 + (eV/2)^2 + \Gamma^2]}{\pi[(B+eV/2)^2 + \Gamma^2][(B-eV/2)^2 + \Gamma^2]}$. The expression for susceptibility in the nonequilibrium state differs slightly from that in Ref. [32]. In isolated limit ($\Gamma \rightarrow 0$) the expressions for equilibrium reduce to $M(B, T) = \frac{1}{2} \tanh\left(\frac{B}{2T}\right)$, the Brillouin function as generally known and $\chi(B, T) = \frac{1}{4T} \operatorname{sech}^2\left(\frac{B}{2T}\right)$. Additionally, in the nonequilibrium state ($\mu_L = -\mu_R = eV/2$, $\Gamma_L = \Gamma_R = \Gamma$), $M(B, T, eV) = \frac{1}{4} \left[\tanh\left(\frac{B+eV/2}{2T}\right) + \tanh\left(\frac{B-eV/2}{2T}\right) \right]$ and $\chi(B, T, eV) = \frac{1}{8T} \left[\operatorname{sech}^2\left(\frac{B+eV/2}{2T}\right) + \operatorname{sech}^2\left(\frac{B-eV/2}{2T}\right) \right]$. The expression for susceptibility in the nonequilibrium state is different somewhat from that in Ref. [32].

In summary, the spectral function based on the nonequilibrium perturbation theory up to the fourth-order is shown for the symmetric Anderson model and the characteristic of the Kondo resonance is investigated for nonequilibrium state due to bias voltage. It is made the improvement of the definition in the Keldysh formalism and then the third-order and the fourth-order contributions to the retarded and advanced self-energies are formulated. From the consequence, it is concluded that the nonequilibrium (real-time) perturbative expansion generalized can be related to the Matubara imaginary-time perturbative expansion for equilibrium. In spectral function, the Kondo peak disappears as bias voltage exceeding the Kondo temperature. this characteristic has been observed by the recent experiment. The present results suggest that the Kondo resonance can be destroyed owing to fluctuation of the Fermi level in nonequilibrium state.

Acknowledgments

The author would like to thank Dr. V. Zlatić for invaluable advice. The numerical calculations were performed at the Yukawa Institute Computer Facility. Additionally, the multiple integrals were executed using the computer subroutine, *MQFSRD* of NUMPAC.

Appendix

The twelve terms for the fourth-order contribution can be divided into four groups, each of which is composed of three terms. The four groups are brought from diagrams denoted in Figs. 4 (a)-(c), Figs. 4 (d)-(f), Figs. 4 (g)-(i), and Figs. 4 (j)-(l), respectively. The terms for the diagrams illustrated in Figs. 4(a) and 4(b) are equivalent except for the spin indices and expressed by

$$\begin{aligned} \Sigma_{a,b}^{r(4)}(E) = & U^4 \int_0^\infty dt_1 \int_{-\infty}^\infty dt_2 \int_{-\infty}^\infty dt_3 e^{iEt_1} \\ & \times \left[\begin{array}{l} g^<(t_1)g^<(t_1 - t_2 - t_3)g^>(-t_1 + t_2 + t_3) \\ -g^>(t_1)g^>(t_1 - t_2 - t_3)g^<(-t_1 + t_2 + t_3) \end{array} \right] \\ & \times \left[\begin{array}{l} g^\pm(t_2)g^<(-t_2) + g^<(t_2)g^\pm(-t_2) \\ g^\pm(t_3)g^<(-t_3) + g^<(t_3)g^\pm(-t_3) \end{array} \right], \end{aligned} \quad (28)$$

$$\begin{aligned}
 \Sigma_{a,b}^{a(4)}(E) = & U^4 \int_{-\infty}^0 dt_1 \int_{-\infty}^{\infty} dt_2 \int_{-\infty}^{\infty} dt_3 e^{iEt_1} \\
 & \times \left[\begin{array}{l} g^>(t_1)g^>(t_1 - t_2 - t_3)g^<(-t_1 + t_2 + t_3) \\ -g^<(t_1)g^<(t_1 - t_2 - t_3)g^>(-t_1 + t_2 + t_3) \end{array} \right] \\
 & \times \left[\begin{array}{l} g^{\pm}(t_2)g^<(-t_2) + g^<(t_2)g^{\pm}(-t_2) \end{array} \right] \\
 & \times \left[\begin{array}{l} g^{\pm}(t_3)g^<(-t_3) + g^<(t_3)g^{\pm}(-t_3) \end{array} \right]. \tag{29}
 \end{aligned}$$

Additionally, Figure 4(c) shows the diagram for the following terms:

$$\begin{aligned}
 \Sigma_c^{r(4)}(E) = & U^4 \int_0^{\infty} dt_1 \int_{-\infty}^{\infty} dt_2 \int_{-\infty}^{\infty} dt_3 e^{iEt_1} \\
 & \times \left[\begin{array}{l} g^>(-t_1)g^<(t_1 - t_2 - t_3)g^<(t_1 - t_2 - t_3) \\ -g^<(-t_1)g^>(t_1 - t_2 - t_3)g^>(t_1 - t_2 - t_3) \end{array} \right] \\
 & \times \left[\begin{array}{l} g^{\pm}(t_2)g^>(t_2) + g^<(t_2)g^{\pm}(t_2) \end{array} \right] \\
 & \times \left[\begin{array}{l} g^{\pm}(t_3)g^>(t_3) + g^<(t_3)g^{\pm}(t_3) \end{array} \right], \tag{30}
 \end{aligned}$$

$$\begin{aligned}
 \Sigma_c^{a(4)}(E) = & U^4 \int_{-\infty}^0 dt_1 \int_{-\infty}^{\infty} dt_2 \int_{-\infty}^{\infty} dt_3 e^{iEt_1} \\
 & \times \left[\begin{array}{l} g^<(-t_1)g^>(t_1 - t_2 - t_3)g^>(t_1 - t_2 - t_3) \\ -g^>(-t_1)g^<(t_1 - t_2 - t_3)g^<(t_1 - t_2 - t_3) \end{array} \right] \\
 & \times \left[\begin{array}{l} g^{\pm}(t_2)g^>(t_2) + g^<(t_2)g^{\pm}(t_2) \end{array} \right] \\
 & \times \left[\begin{array}{l} g^{\pm}(t_3)g^>(t_3) + g^<(t_3)g^{\pm}(t_3) \end{array} \right]. \tag{31}
 \end{aligned}$$

Next, the terms brought from diagram in Fig. 4(d) are expressed by

$$\begin{aligned}
 \Sigma_d^{r(4)}(E) = & U^4 \int_0^{\infty} dt_1 \int_{-\infty}^{\infty} dt_2 \int_{-\infty}^{\infty} dt_3 e^{iEt_1} \\
 & \times \left[\begin{array}{l} g^>(t_1 - t_3)g^>(t_1 - t_2)g^<(t_2 - t_1) \\ -g^<(t_1 - t_3)g^<(t_1 - t_2)g^>(t_2 - t_1) \end{array} \right] \\
 & \times g^{\pm}(t_2) \operatorname{sgn}(t_3) \left[\begin{array}{l} g^>(-t_2 + t_3)g^>(t_3)g^<(-t_3) \\ -g^<(-t_2 + t_3)g^<(t_3)g^>(-t_3) \end{array} \right], \tag{32}
 \end{aligned}$$

$$\begin{aligned}
 \Sigma_d^{a(4)}(E) = & U^4 \int_{-\infty}^0 dt_1 \int_{-\infty}^{\infty} dt_2 \int_{-\infty}^{\infty} dt_3 e^{iEt_1} \\
 & \times \left[\begin{array}{l} g^<(t_1 - t_3)g^<(t_1 - t_2)g^>(t_2 - t_1) \\ -g^>(t_1 - t_3)g^>(t_1 - t_2)g^<(t_2 - t_1) \end{array} \right] \\
 & \times g^{\pm}(t_2) \operatorname{sgn}(t_3) \left[\begin{array}{l} g^>(-t_2 + t_3)g^>(t_3)g^<(-t_3) \\ -g^<(-t_2 + t_3)g^<(t_3)g^>(-t_3) \end{array} \right]. \tag{33}
 \end{aligned}$$

The terms for diagram in Fig. 4(e) are written by

$$\begin{aligned}
 \Sigma_e^{r(4)}(E) = & U^4 \int_0^{\infty} dt_1 \int_{-\infty}^{\infty} dt_2 \int_{-\infty}^{\infty} dt_3 e^{iEt_1} \\
 & \times \left[\begin{array}{l} g^>(t_1 - t_2)g^>(t_1 - t_2)g^<(t_3 - t_1) \\ -g^<(t_1 - t_2)g^<(t_1 - t_2)g^>(t_3 - t_1) \end{array} \right]
 \end{aligned}$$

$$\times g^\pm(t_2) \operatorname{sgn}(t_3) \begin{bmatrix} g^>(t_2 - t_3)g^>(-t_3)g^<(t_3) \\ -g^<(t_2 - t_3)g^<(-t_3)g^>(t_3) \end{bmatrix}, \quad (34)$$

$$\begin{aligned} \Sigma_e^{a(4)}(E) = & U^4 \int_{-\infty}^0 dt_1 \int_{-\infty}^{\infty} dt_2 \int_{-\infty}^{\infty} dt_3 e^{iEt_1} \\ & \times \begin{bmatrix} g^<(t_1 - t_2)g^<(t_1 - t_2)g^>(t_3 - t_1) \\ -g^>(t_1 - t_2)g^>(t_1 - t_2)g^<(t_3 - t_1) \end{bmatrix} \\ & \times g^\pm(t_2) \operatorname{sgn}(t_3) \begin{bmatrix} g^>(t_2 - t_3)g^>(-t_3)g^<(t_3) \\ -g^<(t_2 - t_3)g^<(-t_3)g^>(t_3) \end{bmatrix}. \end{aligned} \quad (35)$$

In addition, Figure 4(f) denotes the diagram for the following terms:

$$\begin{aligned} \Sigma_f^{r(4)}(E) = & U^4 \int_0^{\infty} dt_1 \int_{-\infty}^{\infty} dt_2 \int_{-\infty}^{\infty} dt_3 e^{iEt_1} \\ & \times \begin{bmatrix} g^>(t_1 - t_3)g^>(t_1 - t_2)g^<(t_2 - t_1) \\ -g^<(t_1 - t_3)g^<(t_1 - t_2)g^>(t_2 - t_1) \end{bmatrix} \\ & \times g^\pm(-t_2) \operatorname{sgn}(t_3) \begin{bmatrix} g^<(t_3)g^<(t_3)g^>(t_2 - t_3) \\ -g^>(t_3)g^>(t_3)g^<(t_2 - t_3) \end{bmatrix}, \end{aligned} \quad (36)$$

$$\begin{aligned} \Sigma_f^{a(4)}(E) = & U^4 \int_{-\infty}^0 dt_1 \int_{-\infty}^{\infty} dt_2 \int_{-\infty}^{\infty} dt_3 e^{iEt_1} \\ & \times \begin{bmatrix} g^<(t_1 - t_3)g^<(t_1 - t_2)g^>(t_2 - t_1) \\ -g^>(t_1 - t_3)g^>(t_1 - t_2)g^<(t_2 - t_1) \end{bmatrix} \\ & \times g^\pm(-t_2) \operatorname{sgn}(t_3) \begin{bmatrix} g^<(t_3)g^<(t_3)g^>(t_2 - t_3) \\ -g^>(t_3)g^>(t_3)g^<(t_2 - t_3) \end{bmatrix}. \end{aligned} \quad (37)$$

Next, the terms formulated from diagram illustrated in Fig. 4(g) are expressed by

$$\begin{aligned} \Sigma_g^{r(4)}(E) = & U^4 \int_0^{\infty} dt_1 \int_{-\infty}^{\infty} dt_2 \int_{-\infty}^{\infty} dt_3 e^{iEt_1} \\ & \times \begin{bmatrix} g^>(t_1)g^>(t_1 - t_2 - t_3)g^<(t_2 - t_1) \\ -g^<(t_1)g^<(t_1 - t_2 - t_3)g^>(t_2 - t_1) \end{bmatrix} \\ & \times g^\pm(-t_2) \operatorname{sgn}(t_3) \begin{bmatrix} g^>(t_2 + t_3)g^>(t_3)g^<(-t_3) \\ -g^<(t_2 + t_3)g^<(t_3)g^>(-t_3) \end{bmatrix}, \end{aligned} \quad (38)$$

$$\begin{aligned} \Sigma_g^{a(4)}(E) = & U^4 \int_{-\infty}^0 dt_1 \int_{-\infty}^{\infty} dt_2 \int_{-\infty}^{\infty} dt_3 e^{iEt_1} \\ & \times \begin{bmatrix} g^<(t_1)g^<(t_1 - t_2 - t_3)g^>(t_2 - t_1) \\ -g^>(t_1)g^>(t_1 - t_2 - t_3)g^<(t_2 - t_1) \end{bmatrix} \\ & \times g^\pm(-t_2) \operatorname{sgn}(t_3) \begin{bmatrix} g^>(t_2 + t_3)g^>(t_3)g^<(-t_3) \\ -g^<(t_2 + t_3)g^<(t_3)g^>(-t_3) \end{bmatrix}. \end{aligned} \quad (39)$$

Figure 4(h) illustrates the diagram for the following terms:

$$\begin{aligned} \Sigma_h^{r(4)}(E) = & U^4 \int_0^{\infty} dt_1 \int_{-\infty}^{\infty} dt_2 \int_{-\infty}^{\infty} dt_3 e^{iEt_1} \\ & \times \begin{bmatrix} g^<(t_1)g^<(t_1 - t_2 - t_3)g^>(t_2 - t_1) \\ -g^>(t_1)g^>(t_1 - t_2 - t_3)g^<(t_2 - t_1) \end{bmatrix} \end{aligned}$$

$$\times g^\pm(t_2) \operatorname{sgn}(t_3) \begin{bmatrix} g^>(t_3)g^>(t_3)g^<(-t_2-t_3) \\ -g^<(t_3)g^<(t_3)g^>(-t_2-t_3) \end{bmatrix}, \quad (40)$$

$$\begin{aligned} \Sigma_h^{a(4)}(E) = & U^4 \int_{-\infty}^0 dt_1 \int_{-\infty}^{\infty} dt_2 \int_{-\infty}^{\infty} dt_3 e^{iEt_1} \\ & \times \begin{bmatrix} g^>(t_1)g^>(t_1-t_2-t_3)g^<(t_2-t_1) \\ -g^<(t_1)g^<(t_1-t_2-t_3)g^>(t_2-t_1) \end{bmatrix} \\ & \times g^\pm(t_2) \operatorname{sgn}(t_3) \begin{bmatrix} g^>(t_3)g^>(t_3)g^<(-t_2-t_3) \\ -g^<(t_3)g^<(t_3)g^>(-t_2-t_3) \end{bmatrix}. \end{aligned} \quad (41)$$

Besides, the terms formulated from the diagram in Fig. 4(i) are written by

$$\begin{aligned} \Sigma_i^{r(4)}(E) = & U^4 \int_0^\infty dt_1 \int_{-\infty}^{\infty} dt_2 \int_{-\infty}^{\infty} dt_3 e^{iEt_1} \\ & \times \begin{bmatrix} g^>(-t_1)g^<(t_1-t_2-t_3)g^<(t_1-t_2) \\ -g^<(-t_1)g^>(t_1-t_2-t_3)g^>(t_1-t_2) \end{bmatrix} \\ & \times g^\pm(t_2) \operatorname{sgn}(t_3) \begin{bmatrix} g^>(t_2+t_3)g^>(t_3)g^<(-t_3) \\ -g^<(t_2+t_3)g^<(t_3)g^>(-t_3) \end{bmatrix}, \end{aligned} \quad (42)$$

$$\begin{aligned} \Sigma_i^{a(4)}(E) = & U^4 \int_{-\infty}^0 dt_1 \int_{-\infty}^{\infty} dt_2 \int_{-\infty}^{\infty} dt_3 e^{iEt_1} \\ & \times \begin{bmatrix} g^<(-t_1)g^>(t_1-t_2-t_3)g^>(t_1-t_2) \\ -g^>(-t_1)g^<(t_1-t_2-t_3)g^<(t_1-t_2) \end{bmatrix} \\ & \times g^\pm(t_2) \operatorname{sgn}(t_3) \begin{bmatrix} g^>(t_2+t_3)g^>(t_3)g^<(-t_3) \\ -g^<(t_2+t_3)g^<(t_3)g^>(-t_3) \end{bmatrix}. \end{aligned} \quad (43)$$

Next, the terms for diagrams denoted in Figs. 4 (j) and 4(k) are equivalent except for the spin indices and written by

$$\begin{aligned} \Sigma_{j,k}^{r(4)}(E) = & U^4 \int_0^\infty dt_1 \int_{-\infty}^{\infty} dt_2 \int_{-\infty}^{\infty} dt_3 e^{iEt_1} \\ & \times \begin{bmatrix} g^>(t_1)g^<(-t_1)g^>(t_1-t_2-t_3) \\ -g^<(t_1)g^>(-t_1)g^<(t_1-t_2-t_3) \end{bmatrix} \\ & \times g^\pm(t_2) \begin{bmatrix} g^\pm(t_3)g^>(t_3)g^<(-t_3) \\ +g^<(t_3)g^\pm(t_3)g^>(-t_3) \\ +g^<(t_3)g^>(t_3)g^\pm(-t_3) \end{bmatrix}, \end{aligned} \quad (44)$$

$$\begin{aligned} \Sigma_{j,k}^{a(4)}(E) = & U^4 \int_{-\infty}^0 dt_1 \int_{-\infty}^{\infty} dt_2 \int_{-\infty}^{\infty} dt_3 e^{iEt_1} \\ & \times \begin{bmatrix} g^<(t_1)g^>(-t_1)g^<(t_1-t_2-t_3) \\ -g^>(t_1)g^<(-t_1)g^>(t_1-t_2-t_3) \end{bmatrix} \\ & \times g^\pm(t_2) \begin{bmatrix} g^\pm(t_3)g^>(t_3)g^<(-t_3) \\ +g^<(t_3)g^\pm(t_3)g^>(-t_3) \\ +g^<(t_3)g^>(t_3)g^\pm(-t_3) \end{bmatrix}. \end{aligned} \quad (45)$$

In addition, the terms for diagram illustrated in Fig. 4(l) are expressed by

$$\begin{aligned} \Sigma_l^{r(4)}(E) = & U^4 \int_0^\infty dt_1 \int_{-\infty}^\infty dt_2 \int_{-\infty}^\infty dt_3 e^{iEt_1} \\ & \times \begin{bmatrix} g^>(t_1)g^>(t_1)g^<(-t_1 + t_2 + t_3) \\ -g^<(t_1)g^<(t_1)g^>(-t_1 + t_2 + t_3) \end{bmatrix} \\ & \times g^\pm(-t_2) \begin{bmatrix} g^\pm(-t_3)g^>(-t_3)g^<(t_3) \\ +g^<(-t_3)g^\pm(-t_3)g^>(t_3) \\ +g^<(-t_3)g^>(-t_3)g^\pm(t_3) \end{bmatrix}, \end{aligned} \quad (46)$$

$$\begin{aligned} \Sigma_l^{a(4)}(E) = & U^4 \int_{-\infty}^0 dt_1 \int_{-\infty}^\infty dt_2 \int_{-\infty}^\infty dt_3 e^{iEt_1} \\ & \times \begin{bmatrix} g^<(t_1)g^<(t_1)g^>(-t_1 + t_2 + t_3) \\ -g^>(t_1)g^>(t_1)g^<(-t_1 + t_2 + t_3) \end{bmatrix} \\ & \times g^\pm(-t_2) \begin{bmatrix} g^\pm(-t_3)g^>(-t_3)g^<(t_3) \\ +g^<(-t_3)g^\pm(-t_3)g^>(t_3) \\ +g^<(-t_3)g^>(-t_3)g^\pm(t_3) \end{bmatrix}. \end{aligned} \quad (47)$$

References

- [1] Kondo J 1964 *Prog. Theor. Phys.* **32** 37
- [2] Nozières P 1974 *J. Low Temp. Phys.* **17** 31
- [3] Wilson K G 1975 *Rev. Mod. Phys.* **47** 773
- [4] Anderson P W 1970 *J. Phys. C: Solid State Phys.* **3** 2436
- [5] Nozières P and Blandin A 1980 *J. Physique* **41** 193
- [6] Affleck I 2005 *J. Phys. Soc. Japan* **74** 56
- [7] Ng T -K and Lee P A 1988 *Phys. Rev. Lett.* **61** 1768
- Glazman L I and Raikh M E 1988 *JETP Lett.* **47** 452
- [8] Goldhaber-Gordon D, Shtrikman H, Mahalu D, Abusch-Magder D, Meirav U and Kastner M A 1998 *Nature* **391** 156
- [9] van der Wiel W G, De Franceschi S, Fujisawa T, Elzerman J M, Tarucha S and Kouwenhoven L P 2000 *Science* **289** 2105
- [10] Haldane F D M 1978 *Phys. Rev. Lett.* **40** 416
- [11] Cronenwett S M, Tjerk H, Oosterkamp T H and Kouwenhoven L P 1998 *Science* **281** 540
- [12] Meir Y, Wingreen N S and Lee P A 1993 *Phys. Rev. Lett.* **70** 2601
- [13] Wingreen N S and Meir Y *Phys. Rev. B* **1994** **49** 11040
- [14] Rosch A, Kroha J and Wölfle P 2001 *Phys. Rev. Lett.* **87** 156802
- [15] Fujii T and Ueda K 2003 *Phys. Rev. B* **68** 155310
- [16] Nygård J, Koehl W F, Mason N, DiCarlo L and Marcus C M *Preprint cond-mat/0410467*
- [17] Schwinger J 1961 *J. Math. Phys.* **2** 407
- [18] Keldysh L V 1965 *Sov. Phys.-JETP* **20** 1018
- [19] Yosida K and Yamada K 1970 *Prog. Theor. Phys. Suppl.* **46** 244
- [20] Hershfield S, Davies J H and Wilkins J W 1992 *Phys. Rev. B* **46** 7046
- [21] Oguri A 2002 *J. Phys. Soc. Japan* **71** 2969
- [22] Zlatić V, Horvatić B, Dolički B, Grabowski S, Entel P and Schotte K-D 2000 *Phys. Rev. B* **63** 35104
- [23] Okiji A 1988 *Fermi Surface Effects* edited by Kondo J and Yoshimori A (Springer)
- [24] Lifshitz E M and Pitaevskii L P 1981 *Physical Kinetics* (Pergamon Press)
- [25] Zagoskin A 1998 *Quantum Theory of Many-Body Systems* (Springer-Verlag)

- [26] Caroli C, Combescot R, Nozières P and Saint-James D 1971 *J. Phys. C: Solid State Phys.* **4** 916
- [27] Huang K 1998 *Quantum Field Theory* (John Wiley & Sons, Inc.)
- [28] Yamada K, 1975 *Prog. Theor. Phys.* **53** 970 ; 1976 *Prog. Theor. Phys.* **55** 1345
- [29] Horvatić B and Zlatić V 1980 *Phys. Stat. Sol. (b)* **99** 251
- [30] Zlatić V and Horvatić B 1983 *Phys. Rev. B* **28** 6904
- [31] Hewson A C 1993 *The Kondo Problem to Heavy Fermions* (Cambridge University Press, Cambridge)
- [32] Coleman P and Mao W 2004 *J. Phys.: Condens. Matter* **16** L263

Fig. 1 The time-contour which starts and ends at $t = -\infty$.

Fig. 2 The diagram for the second-order self-energy. The solid line denotes the noninteracting Green's function and the dashed line denotes interaction.

Figs. 3 (a) (b) The two diagrams for the third-order self-energy.

Figs. 4 (a) (b) (c), Figs. 4 (d) (e) (f), Figs. 4 (g) (h) (i), Figs. 4 (j) (k) (l)
The twelve terms for the proper fourth-order self-energy divided into four groups.

Figs. 5 The second-order self-energy for the symmetric Anderson model at $U/\Gamma = 1.0$ and zero temperature. (a) The real part and (b) The imaginary part at equilibrium (solid line), $eV/\Gamma = 1.0$ (thin solid line), and $eV/\Gamma = 2.0$ (dashed line).

Figs. 6 The fourth-order self-energy for the symmetric Anderson model at $U/\Gamma = 1.0$ and zero temperature. (a) The real part and (b) The imaginary part at equilibrium (solid line), $eV/\Gamma = 1.0$ (thin solid line), and $eV/\Gamma = 2.0$ (dashed line).

Fig. 7 The spectral function with the second-order self-energy at $U/\Gamma = 10.0$ and zero temperature for the symmetric Anderson model at equilibrium (solid line), $eV/\Gamma = 1.0$ (thin solid line) and $eV/\Gamma = 2.0$ (dashed line).

Fig. 8(a) The spectral function with self-energy up to the fourth-order at equilibrium and zero temperature for the symmetric Anderson model at $U/\Gamma = 3.5$ (dashed line) and $U/\Gamma = 5.0$ (solid line).

Fig. 8(b) The spectral function with self-energy up to the fourth-order at $eV/\Gamma = 0.5$ and zero temperature for the symmetric Anderson model at $U/\Gamma = 3.5$ (dashed line) and $U/\Gamma = 5.0$ (solid line).

Fig. 8(c) The spectral function with self-energy up to the fourth-order at $eV/\Gamma = 1.0$ and zero temperature for the symmetric Anderson model at $U/\Gamma = 3.5$ (dashed line) and $U/\Gamma = 5.0$ (solid line).

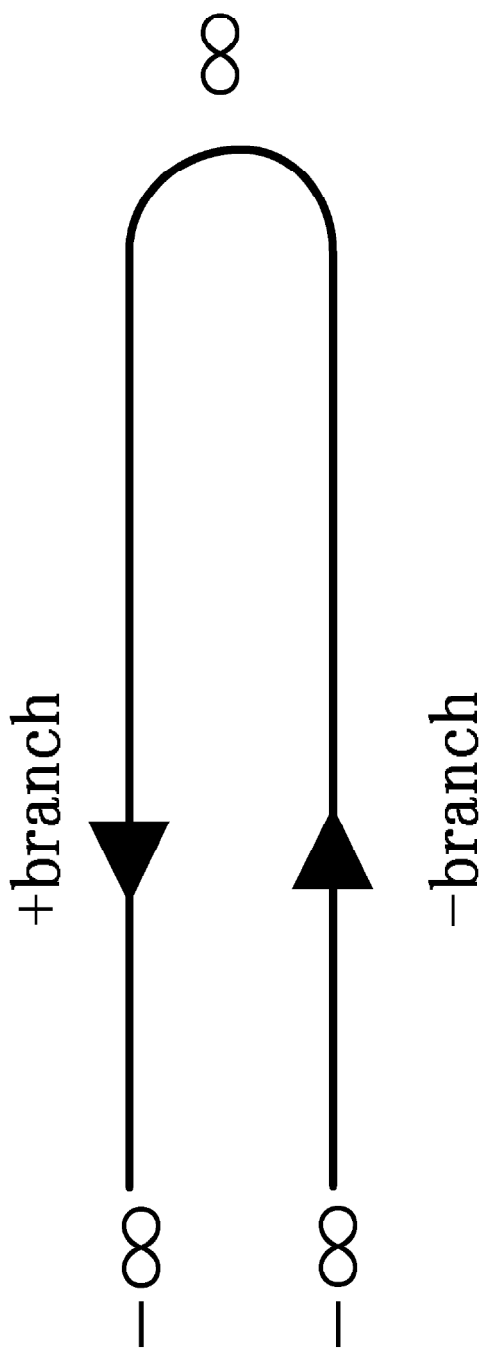


Fig. 1 Hamasaki

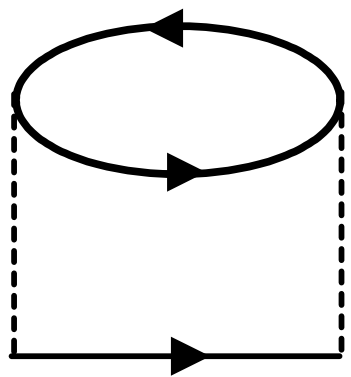


Fig.2 **Hamasaki**

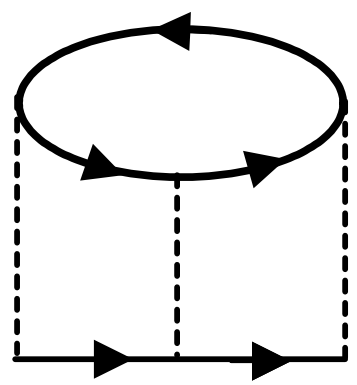


Fig.3(a) Hamasaki

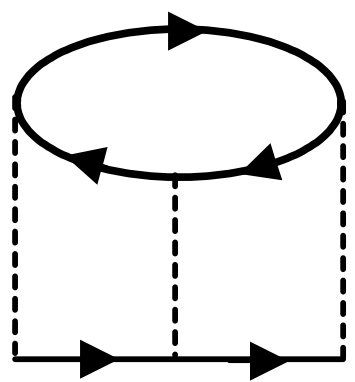


Fig.3(b) Hamasaki

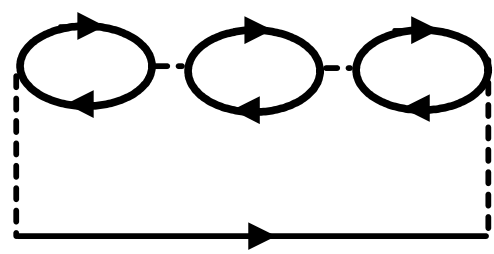


Fig.4(a) Hamasaki

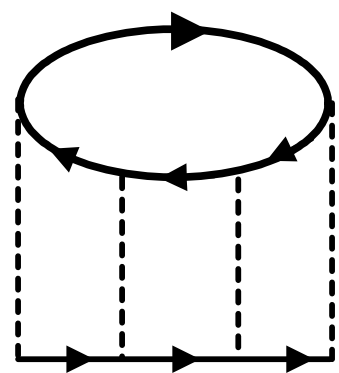


Fig.4(b) Hamasaki

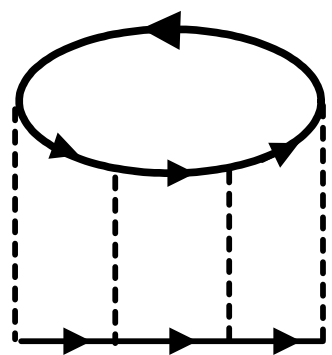


Fig.4(c) Hamasaki

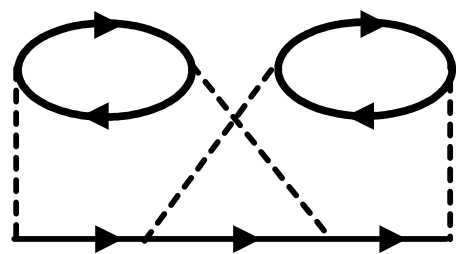


Fig.4(d) hamasaki

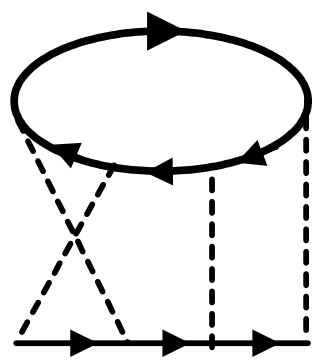


Fig.4(e) Hamasaki

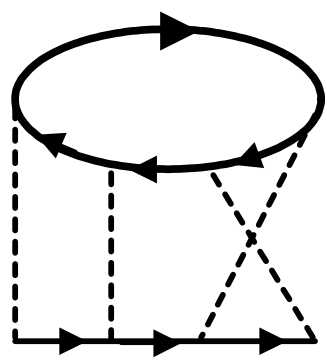


Fig.4(f) Hamasaki

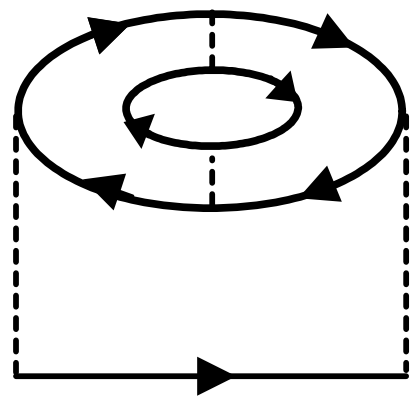


Fig.4(g) Hamasaki

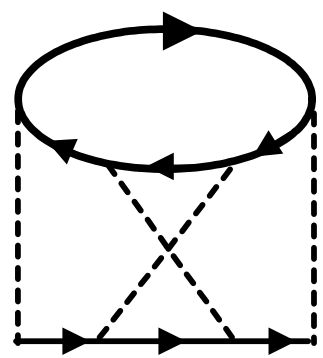


Fig.4(h) Hamasaki

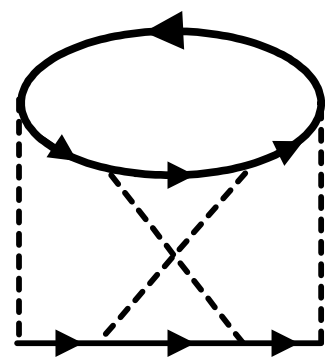


Fig.4(i) Hamasaki

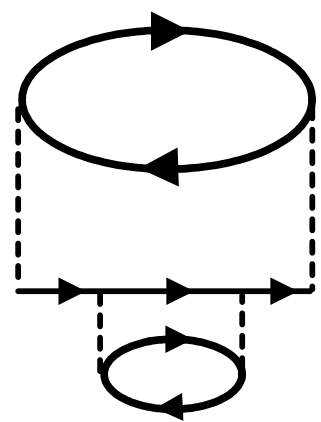


Fig.4(j) Hamasaki

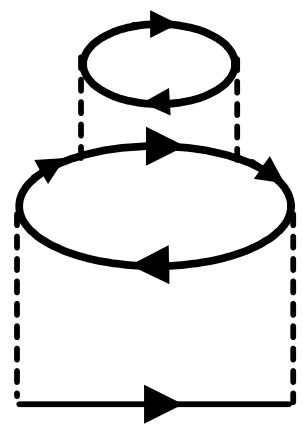


Fig.4(k) Hamasaki

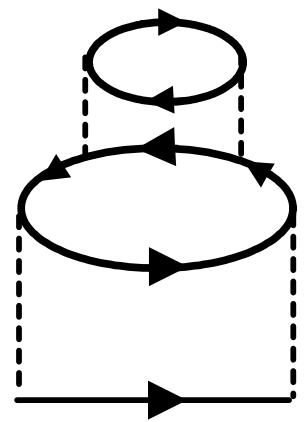


Fig.4(l) Hamasaki

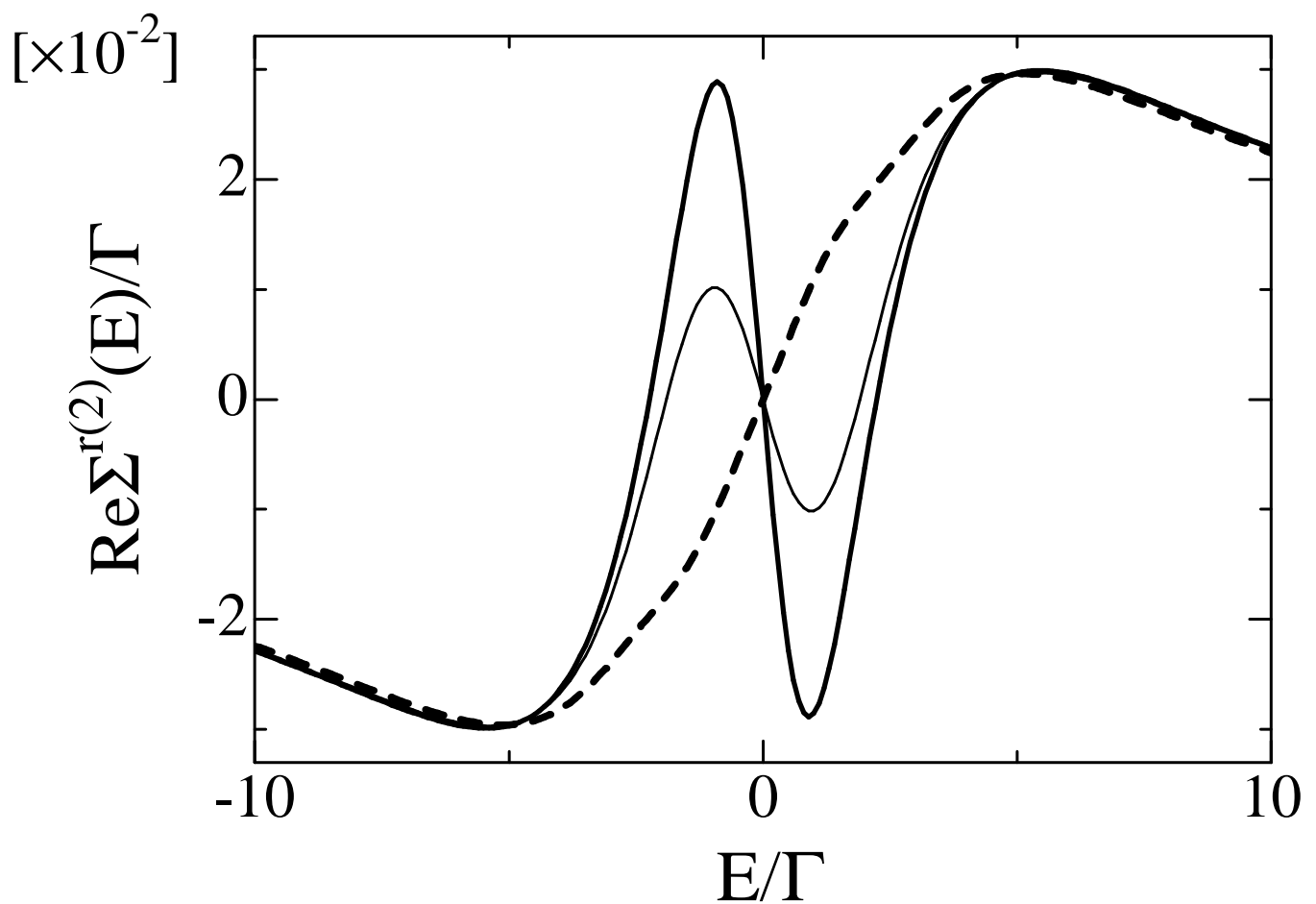


Fig.5(a) Hamasaki

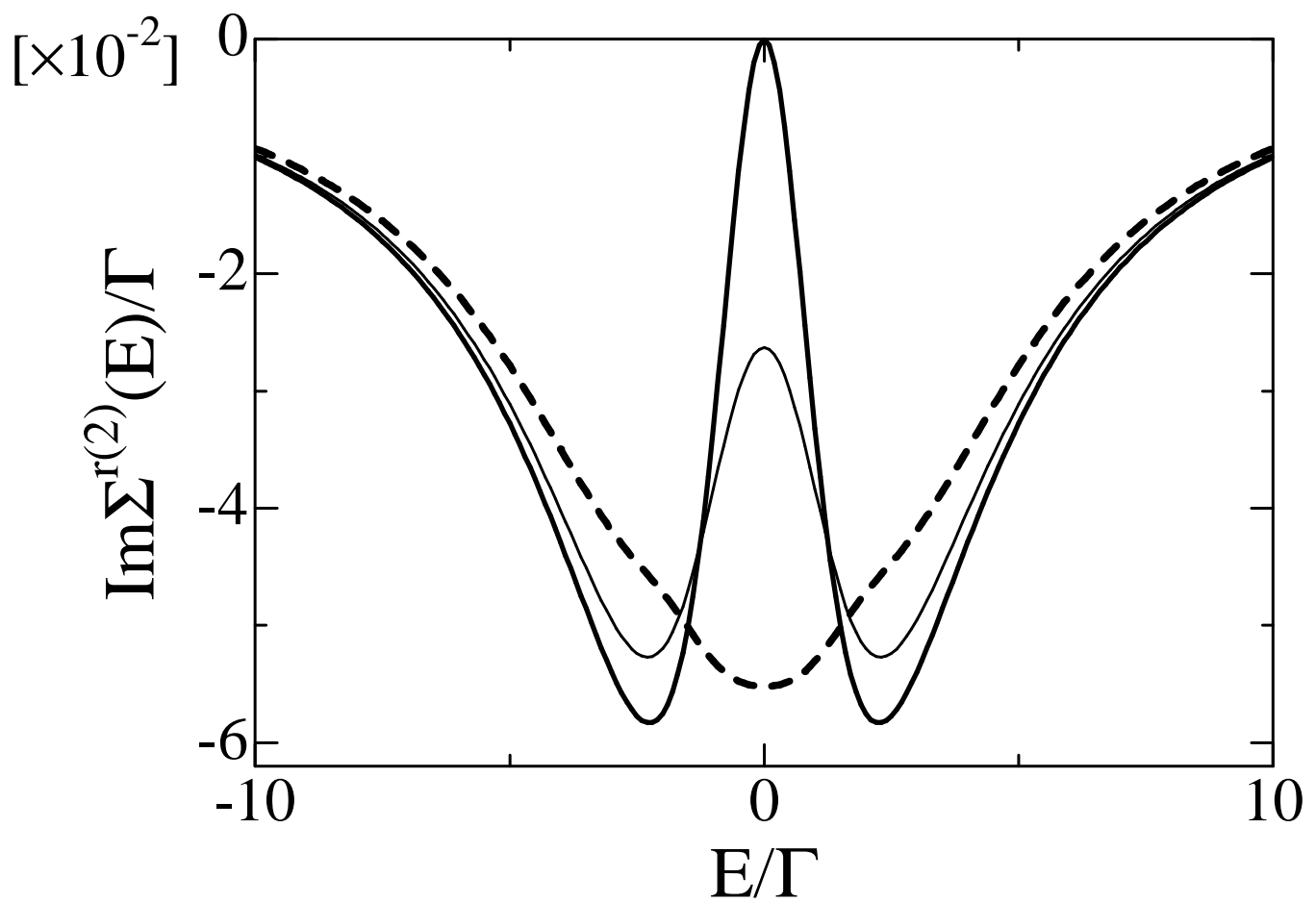


Fig.5(b) Hamasaki

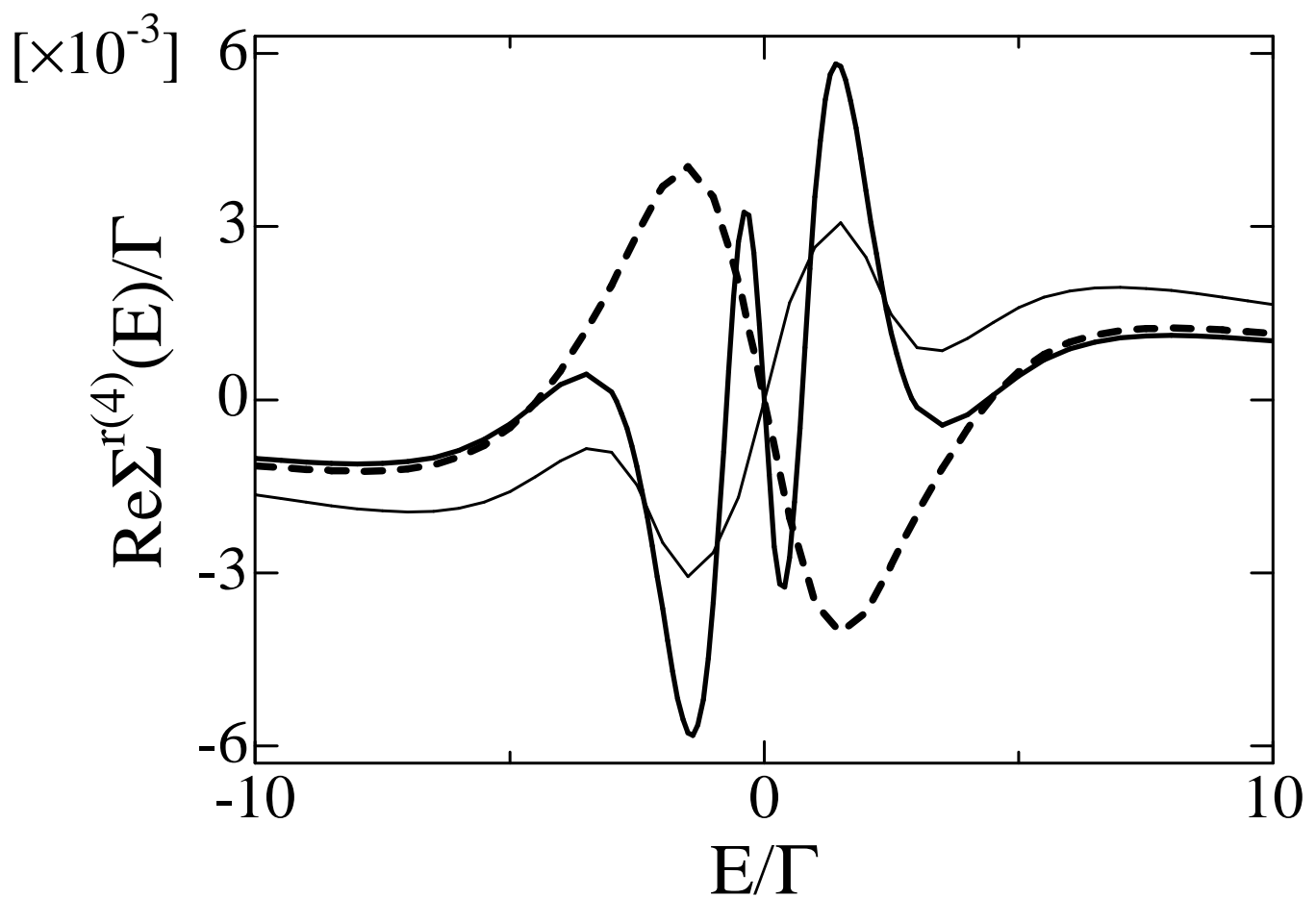


Fig.6(a) Hamasaki

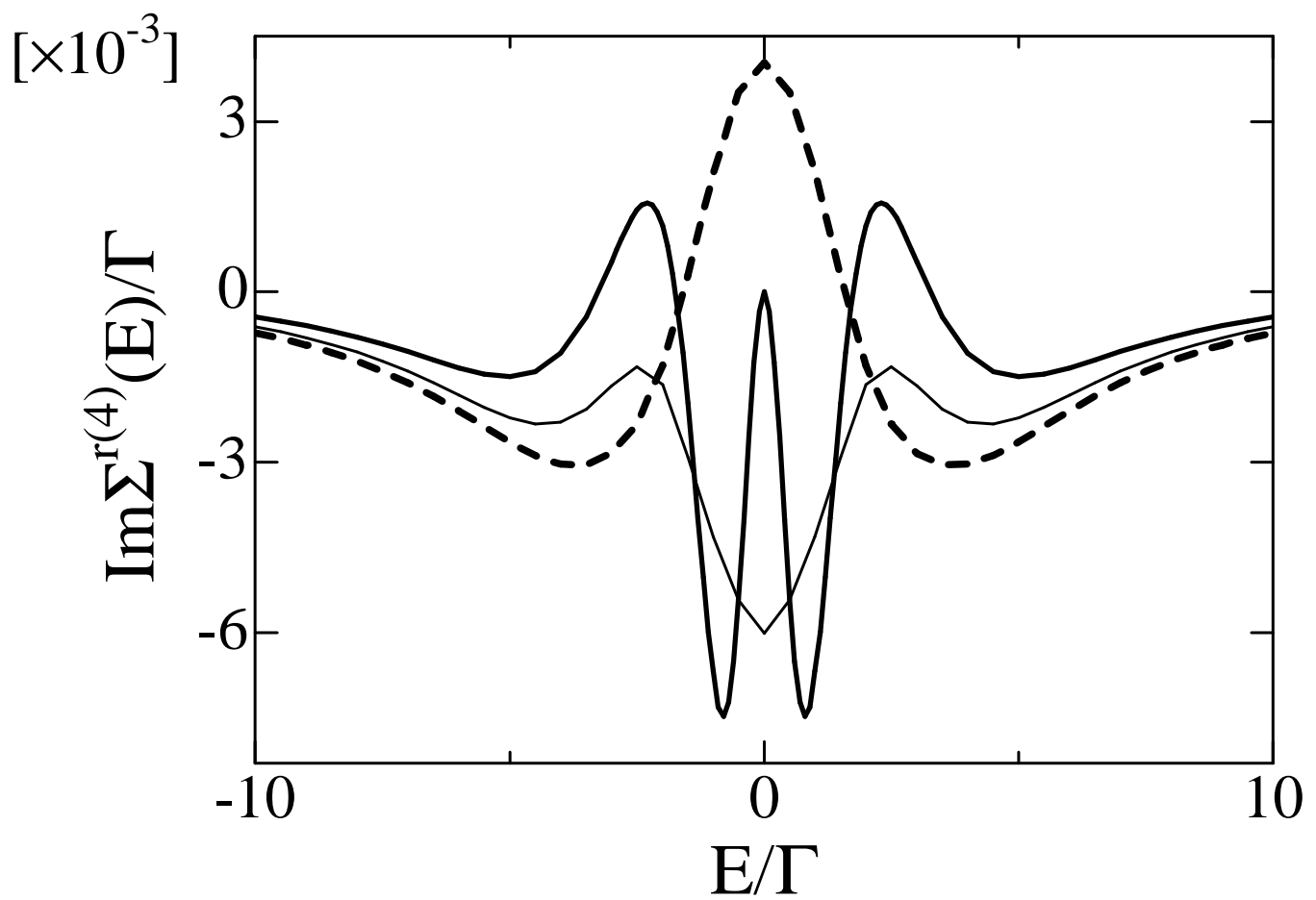


Fig.6(b) Hamasaki

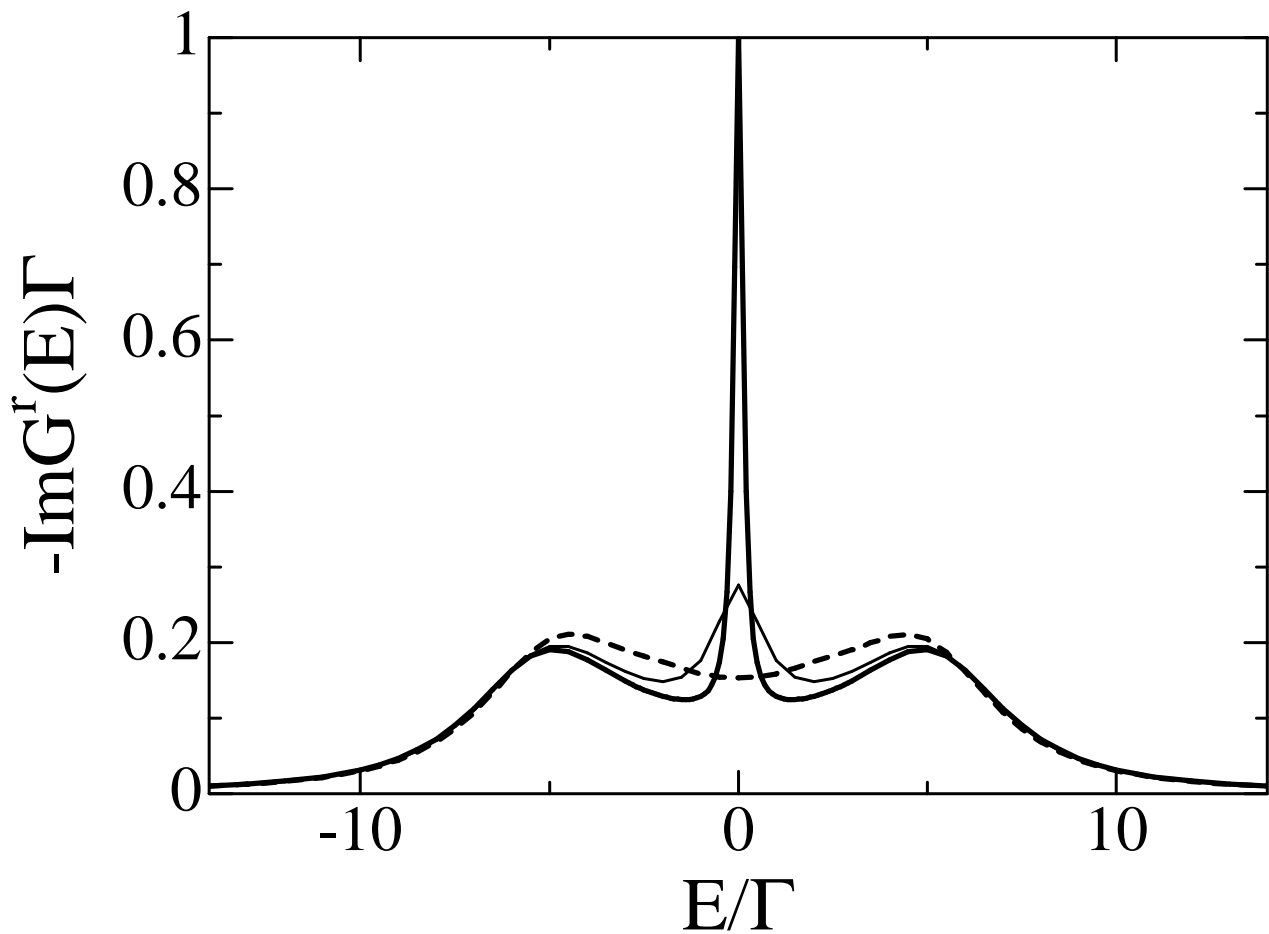


Fig.7 Hamasaki

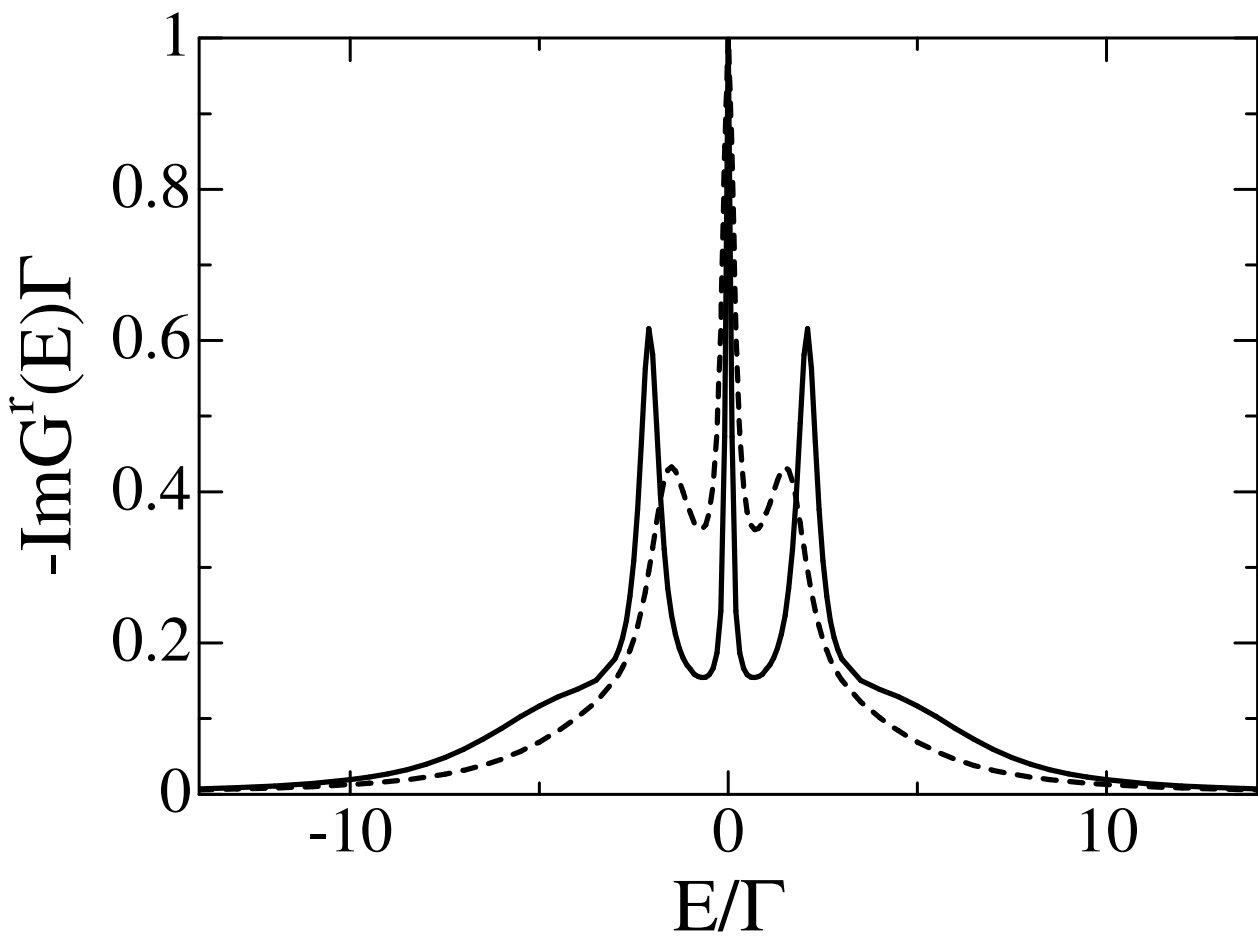


Fig.8(a) Hamasaki

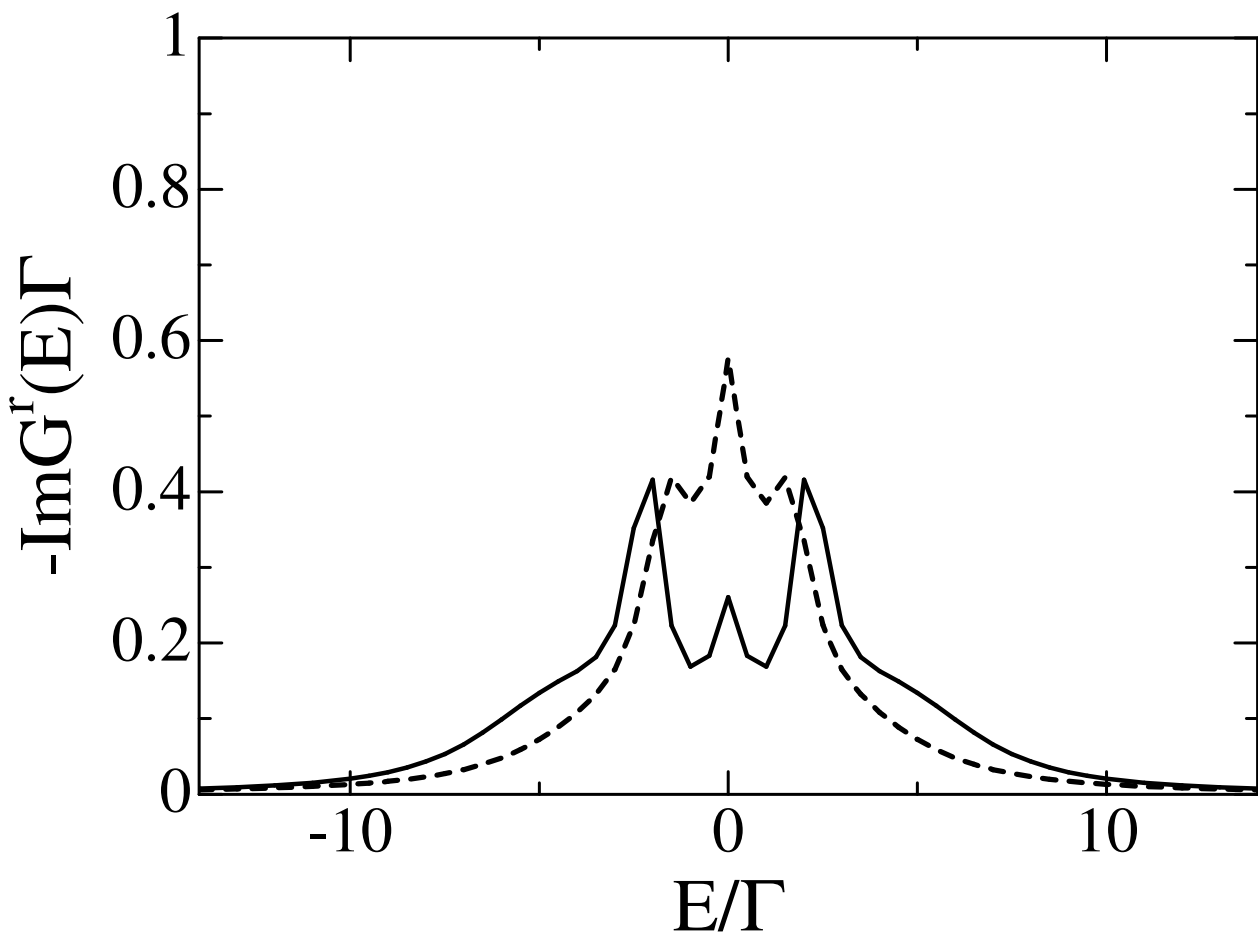


Fig.8(b) Hamasaki

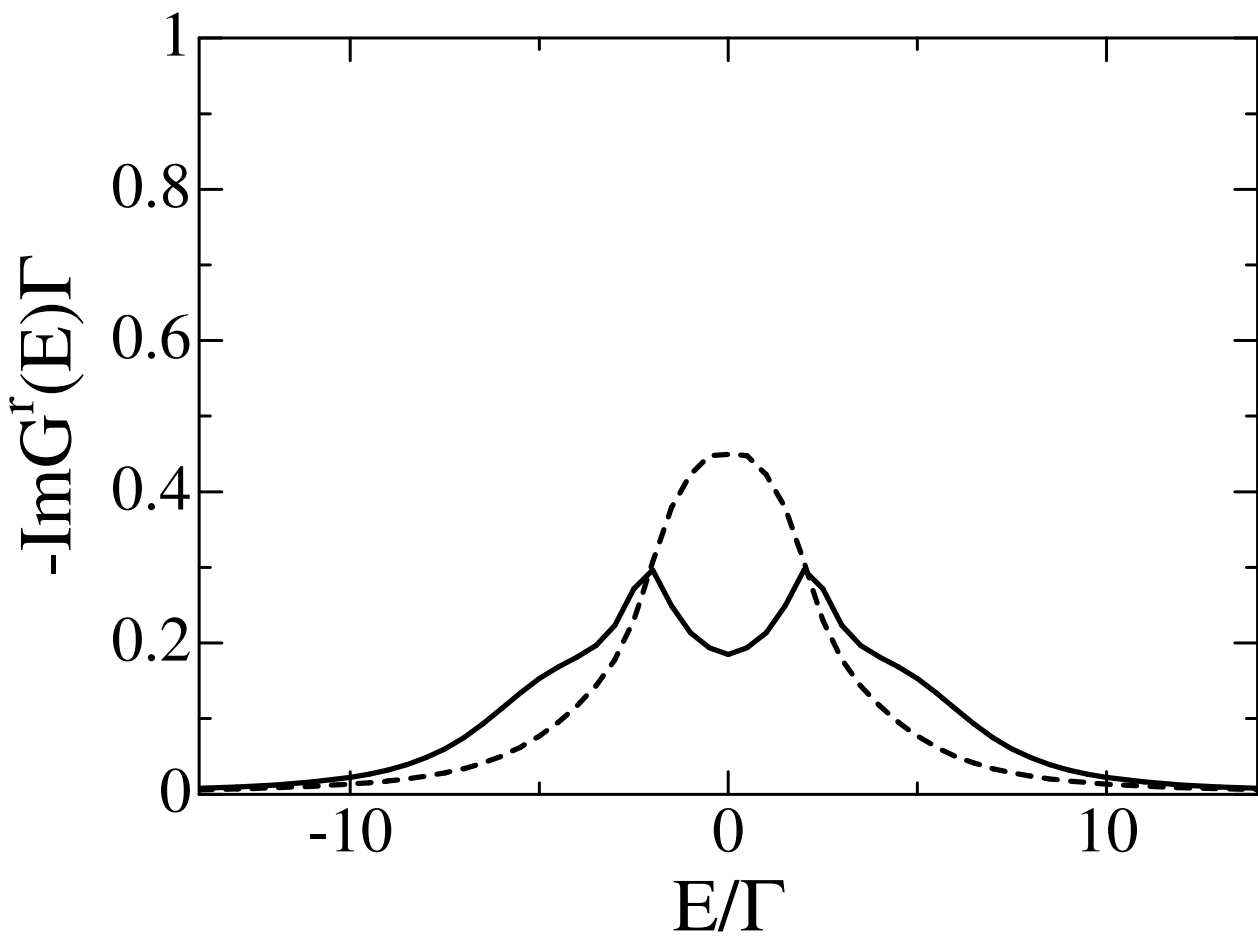


Fig.8(c) Hamasaki

